Fine Structure of Cloud Patterns within the Intraseasonal Oscillation during TOGA COARE

XIAOQING WU AND MARGARET A. LEMONE
National Center for Atmospheric Research, Boulder, Colorado*

(Manuscript received 21 August 1998, in final form 14 December 1998)

ABSTRACT

The relationship of satellite-derived cloud motions to actual convective systems within a convectively active phase of the intraseasonal oscillation is examined by using both cloud-scale properties produced by a cloud-resolving model and field observations to clarify what is going on at shorter time- and space scales. Each convective system has a life cycle of up to 1–2 days. Described in terms of active convection, the system consists of successive precipitation cells generated ahead of the gust front. Described in terms of its cloud shield, the system is more continuous. When easterly winds prevail above 2 km, both precipitating clouds and upper-tropospheric anvil clouds move westward with about the same phase speed ($\sim$10 m s^{-1}). However, during the westerly wind period, precipitating clouds move *eastward* with a phase speed of $\sim$10 m s^{-1}, which is better represented by the radar observations and surface precipitation. The westward movement of cloud patterns viewed from the satellite images is mostly due to the horizontal advection of the anvil by the mean flow and the creation of new convective cells to the west of the old convective clouds.

1. Introduction

Using 3-hourly Geostationary Meteorological Satellite (GMS) infrared (IR) data, Nakazawa (1988) presented a hierarchical structure of intraseasonal (30–60 day) oscillations over the western Pacific. Within the 30–60-day oscillations, several ''super cloud clusters'' near the equator were identified with a horizontal scale of several thousand kilometers and an eastward speed of about 10–15 m s^{-1}. Within a super cloud cluster, several westward-moving cloud clusters were found having a horizontal scale of several hundred kilometers and a timescale of 1–2 days. Similar multiscale convective activity embedded in the 30–60-day oscillation was documented over the western Pacific warm pool in the Northern Hemisphere winter of the First GARP Global Experiment year (e.g., Lau et al. 1991; Sui and Lau 1992) and in the Tropical Ocean Global Atmosphere (TOGA) Coupled Ocean–Atmosphere Response Experiment (COARE) during the westerly wind period (e.g., Takayabu et al. 1996; Chen et al. 1996). Refining the definition of cloud cluster as an enclosed region on a satellite infrared image with temperatures less than 208 K, Chen et al. (1996) noted that Nakazawa's westward-moving ''disturbances'' consisted of several cloud clusters, thus adding a smaller spatial and temporal scale to the hierarchy. It can be seen from Fig. 11 of Chen et al. that some of the clusters in the westward-moving disturbances moved eastward.

Several authors have suggested explanations for these cloud patterns. Lau et al. (1989) related the eastward-moving super cloud clusters and westward-moving cloud clusters to equatorially trapped Kelvin and Rossby wave modes, respectively. Takayabu (1994) interpreted the westward-moving disturbances as a dynamical wave with a 2-day period. Chen et al. (1996) used the fact that the westward-moving disturbances consisted of a sequence of clusters to suggest that the disturbance was a 2-day wave. More recently, Haertel and Johnson (1998) combined satellite, radiosonde, and surface data to strengthen the case for 2-day waves, whose westward propagation they attributed to lowering the level of free convection west of preexisting convection, which favors the development of new convection.

Analysis of radar data from TOGA COARE reveals that convective systems more often move eastward than westward, reinforcing the idea that the westward-propagating disturbances are waves and refining the inter-

* The National Center for Atmospheric Research is sponsored by the National Science Foundation.

Corresponding author address: Dr. Xiaoqing Wu, NCAR, P.O. Box 3000, Boulder, CO 80307.
E-mail: xiaoqing@ncar.ucar.edu

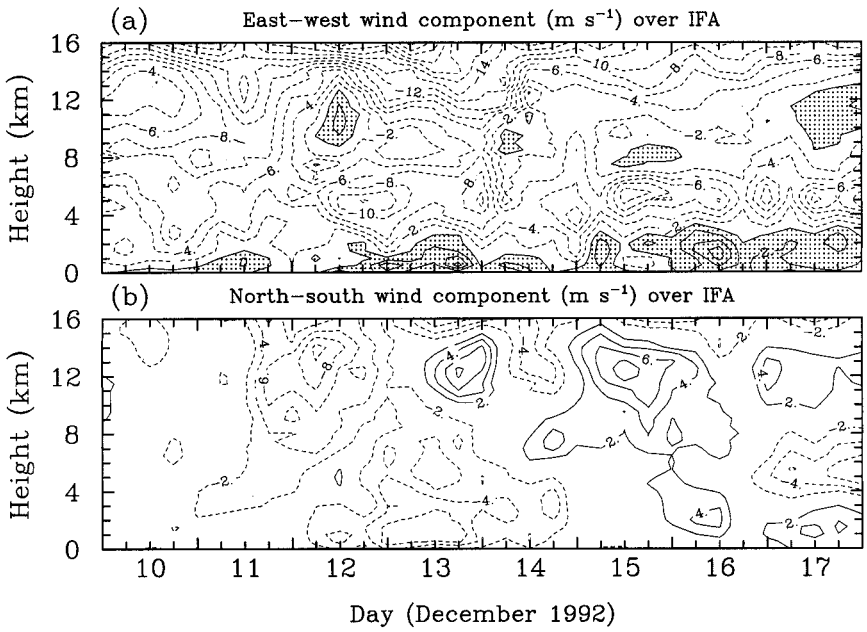

FIG. 1. Evolution of (a) the east–west wind component and (b) the north–south wind component averaged over IFA during 10–17 Dec 1992. Contour intervals are 2 m s^{-1}.

pretation of satellite data at shorter time- and space scales. LeMone et al. (1994) and Rickenbach (1999), manuscript submitted to *Mon. Wea. Rev.*) illustrated that an eastward-moving squall line can have a westward-moving cold cloud top in satellite images. LeMone et al. (1998) found that only a small fraction (4 out of 19) of the mesoscale convective systems documented by the radars on the turboprop aircraft in TOGA COARE moved westward; and three of the four systems that did were associated with low-level easterlies. With low-level westerlies, the systems moved eastward, something that was also observed from the shipboard radar (e.g., Veldon and Young 1994; Rickenbach and Rutledge 1998). In a study of a TOGA COARE mesoscale convective system that occurred in strong low-level westerlies on 10 February, Geldmeier and Barnes (1997)

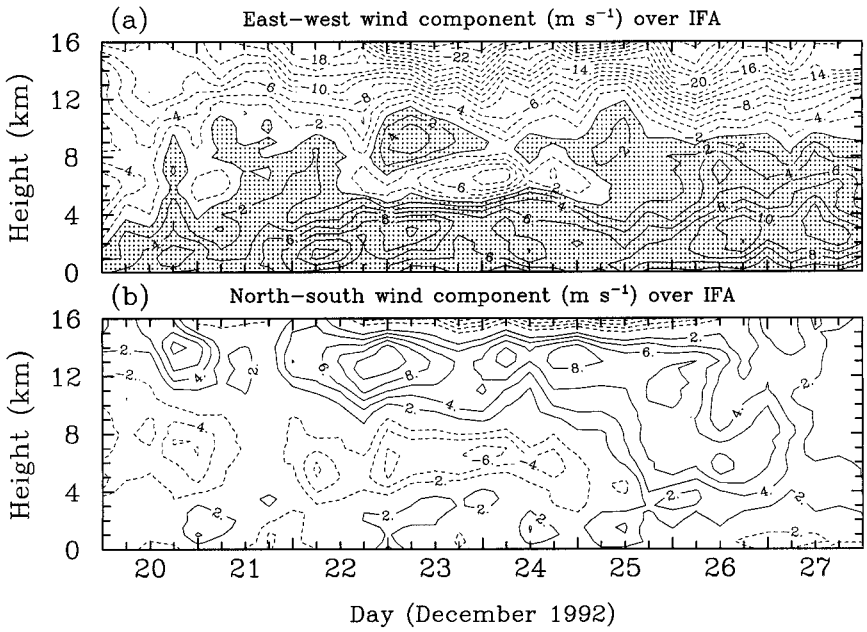

FIG. 2. Same as Fig. 1 except during 20–27 Dec 1992.

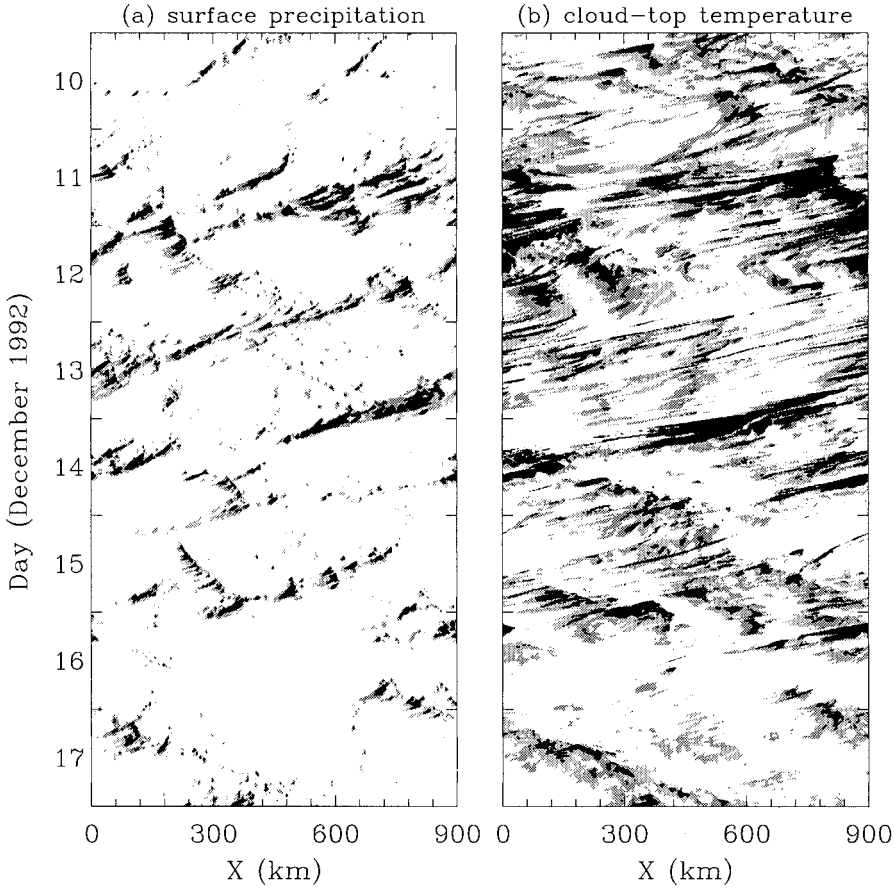

FIG. 3. Hovmöller diagram of (a) the surface rainfall rate and (b) the cloud-top temperature from the model for 10–17 Dec 1992. Light and dark shading in (a) represent precipitation intensity larger than 1 and 5 mm h^{-1}, respectively. Light and dark shading in (b) represent temperature colder than 214 and 208 K, respectively.

noted a similar discrepancy between the motion of precipitation and cloud tops.

Although there now seems to be developing consensus as to the nature of the superclusters and the westward-moving disturbances, understanding what goes on at the shorter time- and space scales requires both satellite data, which represent mainly cloud tops, and radar and aircraft data, which emphasize the convective structure beneath. We propose two reasons for the differences between satellite and radar signatures during the westerly wind period in TOGA COARE: first, the cloud movement seen in satellite images actually represents upper-tropospheric anvil cloud being advected westward from its convective source, particularly when convection is in its late stages or inactive; and second, even if precipitating convective cells move eastward, apparent westward motion seen from space results from new convective cells forming to the west of old convective clouds. In the latter case, one could envision a westward-propagating forcing mechanism of some type, as proposed by Takayabu (1994), Takayabu et al. (1996), Chen et al. (1996), and Haertel and Johnson (1998).

In this paper, we use data from a two-dimensional cloud-resolving model (CRM), airborne radar, and satellite to examine the mechanisms for the movement and organization of the cold cloud tops and the convection beneath. Following Chen et al. (1996), a cloud cluster is defined as a region of contiguous or nearly contiguous cloud that has a temperature colder than 208–214 K. The convection beneath will be defined in terms of radar reflectivity and surface precipitation.

The CRM is that used by Wu et al. (1998, 1999) to diagnose the cloud-scale properties over the intensive flux array (IFA) of TOGA COARE under evolving large-scale conditions for a 39-day period. The CRM domain is 900 km long by 40 km deep with a horizontal grid spacing of 3 km. The CRM explicitly resolves the cloud-scale dynamics and couples many important physical processes (e.g., turbulence, microphysics, radiation, and surface fluxes). The dynamically consistent long-

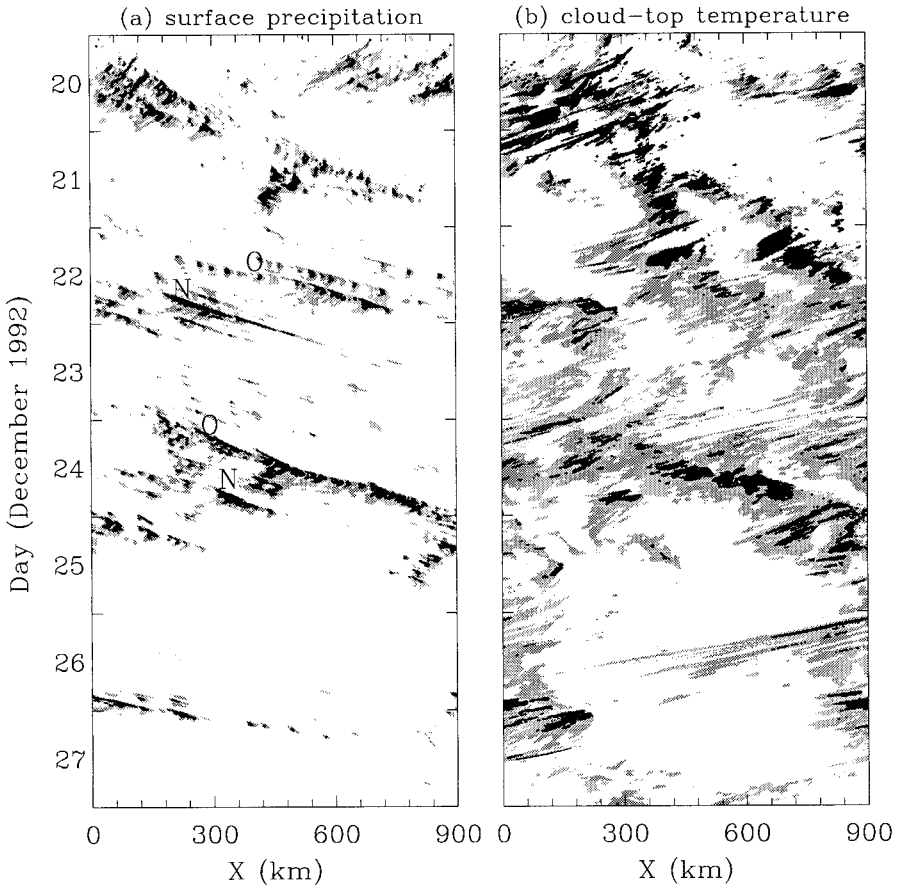

FIG. 4. Same as Fig. 3 except for 20–27 Dec 1992. The letters N and O in (a) represent the new and old convective cells, respectively.

term cloud-scale data produce coherent pictures of upper-tropospheric clouds and precipitating convective clouds over the IFA. Note that the CRM is two-dimensional (2D) at the present time, and a three-dimensional CRM may generate a more complicated picture of cloud movement. TOGA COARE aircraft sampled convective cells using conventional and Doppler radars and in situ data enabling a detailed analysis of precipitating convective clouds (e.g., Yuter et al. 1995; Trier et al. 1997; Jorgensen et al. 1997).

2. Movement of cloud patterns obtained from the CRM

Two periods are selected from the 39-day simulation (Wu et al. 1999), in which a modified ice microphysical scheme was used. Each period has 8 days: the first period is 10–17 December 1992 and the second period is 20–27 December 1992. Both periods are within the convectively active phase of an eastward-propagating intraseasonal oscillation. The large-scale wind fields averaged over the IFA for these two periods are shown in Figs. 1 and 2. During the first period, westerly wind is dominant below 2 km (Fig. 1a), while during the second period, westerly wind is dominant below 5 km (Fig. 2a). Easterly winds prevail at higher levels for both periods. The north–south wind components for both periods are shown in Figs. 1b and 2b, respectively. Both northerly and southerly winds are present in these two periods. Figures 3a and 3b show the evolution of the CRM-produced surface precipitation and cloud-top temperature, respectively, for 10–17 December 1992. The cloud-top temperature is defined as the temperature at the height where the downward-integrated cloud (ice and liquid) water exceeds 3 g m^{-2}. Both heavy precipitation (dark shading in Fig. 3a) and light precipitation (light shading in Fig. 3a) are moving westward. The upper-tropospheric anvil clouds (light shading in Fig. 3b indicates cloud-top temperatures of 208–214 K; dark shading indicates cloud-top temperatures below 208 K) generally move in the same direction as the precipitating clouds with about the same speed of 10 m s^{-1}. As a result, the anvil clouds are not widely spread but overlap the precipitating clouds beneath. The dark streaks in Fig. 3b correspond to cloud clusters as defined by Chen et al. (1996); they can persist as long as a day. Most clus-

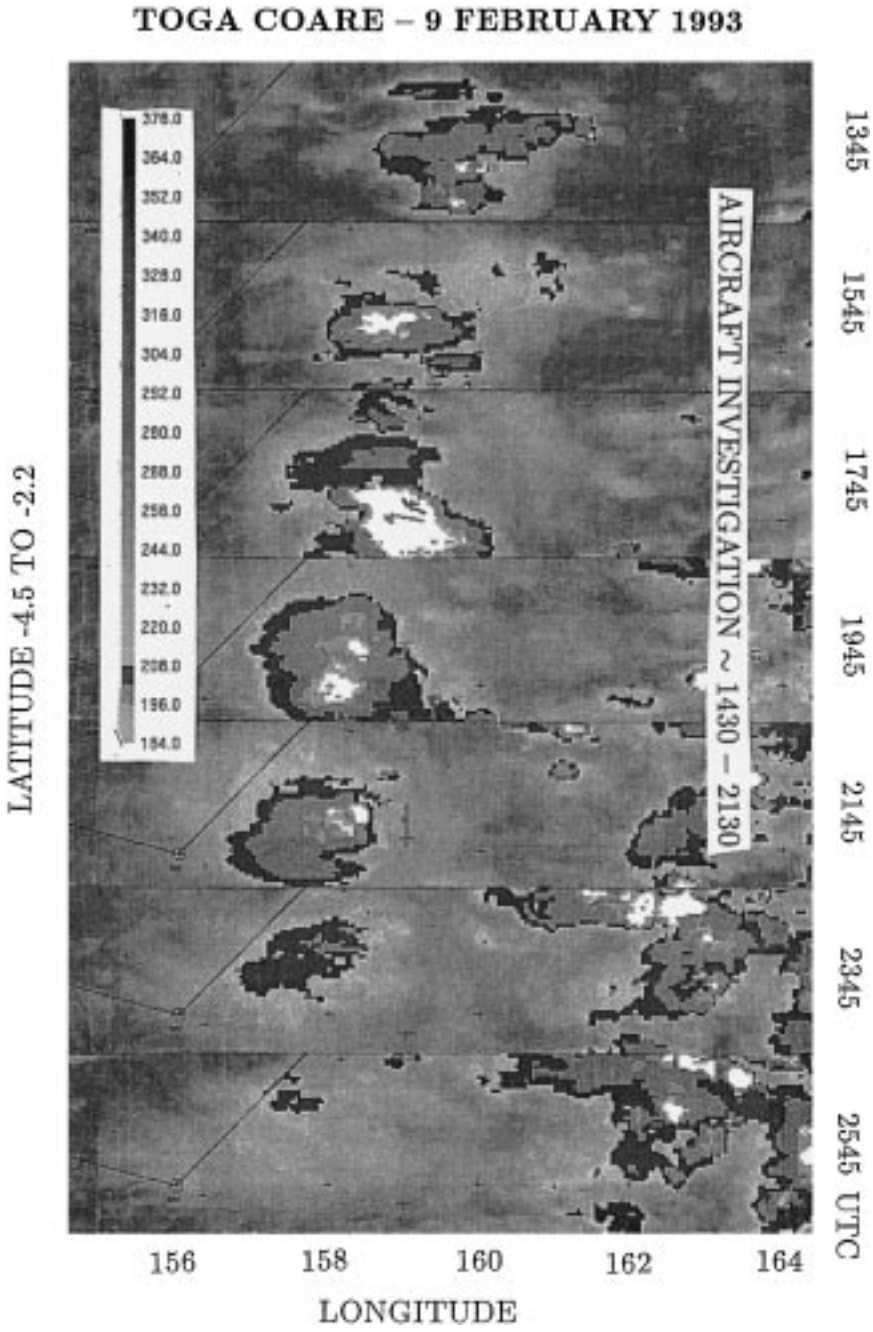

FIG. 5. 9 February GMS satellite IR-based Hovmöller diagram. North–south direction roughly 2.3° lat. Southeast part of IFA outlined. Shorter lines superimposed at and near area of low infrared temperatures are aircraft tracks. The bar at left indicates shading associated with IR temperatures, which is white for temperatures less than 184 K.

ters appear to overlie a series of precipitation cells (dark shading area in Fig. 3a). The movement of precipitating convection during the first period is approximately represented by the satellite-measured cloud movement [see Fig. 9 in Wu et al. (1998)].

However, the cloud-movement pattern during the second period (Fig. 4) is very different from that during the first period, especially for the precipitating convective clouds. The precipitating clouds move eastward (Fig. 4a), while the clusters, as defined by the black and gray streaks in Fig. 4b, move westward. The eastward movement of precipitating clouds is consistent with that measured from radar observations [see Fig. 7 in Wu et al. (1998)]. There are four active periods around 20, 22,

24, and 26 December. Each active period has several sequences of precipitating clouds, in which new cells form east of the old. Each sequence corresponds in the 2D model to a convective band with new cells forming at its leading edge. Each band has a life cycle of up to 1 day and an eastward speed of 10 m s^{-1} (Fig. 4a). The interesting feature is that within these active periods, new bands (see letters N in Fig. 4a) sequentially develop to the west of old bands (see letters O in Fig. 4a), and then move eastward (Fig. 4a). Convergence between the westerly wind and the outflow from the older convective-band mesoscale convective systems and large-scale forcing [strong cooling aloft and strong moistening at lower levels; see Figs. 1a and 1b in Wu et al. (1998)] are responsible for the generation of the new bands. Each convective cell grows upward to feed the westward-moving anvil clouds (Fig. 4b). Due to the strong westerly wind in the lower troposphere and the strong easterly wind in the upper troposphere (i.e., the strong wind shear in the troposphere), anvil debris (cold cloud) from the convective cells is advected westward a long distance relative to the cells as well as relative to the surface (Fig. 4b). The light rain in Fig. 4a moves westward at the same speed as the cloud tops in Fig. 4b. However, the cloud tops also tend to form groups that move eastward with the convective bands, most prominently on 22 and 24 December.

The results shown above suggest that the satellite-measured westward movement of cold cloud tops in westerly wind situations (like those depicted in Fig. 4b) is mainly due to the horizontal advection of upper-tropospheric anvil clouds and the creation of new convective cells to the west of the old convective clouds. The Rossby wave mode and inertio-gravity wave mode that were proposed for the westward movement of cloud clusters in the satellite observations (e.g., Lau et al. 1989; Takayabu 1994; Haertel and Johnson 1998) could explain the previously mentioned large-scale forcing that favors the new convective cells initiated west of the old convective clouds.

3. Movement of cloud patterns observed from the aircraft

a. General behavior

Tracking of 19 convective systems sampled by the three turboprop aircraft during TOGA COARE indicates that the motion of organized mesoscale convective systems, which was related to the low-level wind, was from all points of the compass (LeMone et al. 1998). As for the CRM convective systems, the motion of the observed systems was also strongly related to the low-level wind (e.g., Sui and Lau 1992). The clearest relationship for the observed convection was for the eight convective bands perpendicular to the low-level shear (''shear perpendicular'' bands), which had the characteristics of Moncrieff's (1981) propagating systems. The bands occurred in environments with substantial low-level shear below the low-level wind maximum, moved with the speed of the band-normal component of the low-level wind maximum, and most had trailing stratiform regions. However, there was sometimes substantial motion of convective cells along the bands as well. Such behavior has been documented in many previous observational studies (e.g., Betts et al. 1976; Barnes and Sieckman 1984; Keenan and Carbone 1992).

Only 4 out of these 19 systems had a motion component toward the west. Three of these systems occurred in environments with low-level easterlies, and the fourth occurred in an environment with a shallow layer (below 900 mb) of westerlies and prevailing easterlies above.

b. Comparison of satellite-derived and aircraft-derived convective system motion

We compare the satellite and aircraft radar data for two particularly well-documented convective systems, those of 9 February and 20 February 1993. The results support several points illustrated in the CRM discussion.

1) 9 FEBRUARY CASE

Figure 5 is a GMS satellite IR-based Hovmöller diagram, and Fig. 6 is a sequence of low-level reflectivity maps from the C-Band lower-fuselage radar images from *NOAA-42* of a mesoscale convective system that formed east of the TOGA COARE IFA on 9 February 1993. The system consisted of a long (up to ~300 km) mesoscale band (Smull et al. 1996) with stratiform cloud mainly to the south and southwest (Smull et al. 1994). It formed to the south of a dissipating convective system. The band was normal to the shear below the low-level wind maximum in the environmental wind profile, but parallel to the shear above the wind maximum (LeMone et al. 1998).

The satellite diagram shows a 250-km westward dis-

→

FIG. 6. For 9 February convective system, low-level composite radar reflectivity from the P3 lower-fuselage C-Band radar at hourly intervals. The reflectivity at each point is the maximum value of the reflectivity over the period of the composite (roughly 5 min, centered on the time at left). The lines indicate the aircraft flight tracks. The scale for radar reflectivity (dB*Z*) appears at the bottom. The width of the image is 240 km; the lower-left corner of the image is at 4.879°S and 158.318°E; north is indicated on the figure. Arrows indicate the east end of the convective band of interest. In the top frame, the hand is just forming, south of an extensive area of stratiform precipitation. By 1530 UTC, the cells have formed a roughly east–west line, which reorients to east-southeast to west-northwest by 1625 UTC. The system is stratiform by 1831 UTC. The convective band extends westward farther than the figure implies; its reflectivity is blocked by attenuation.

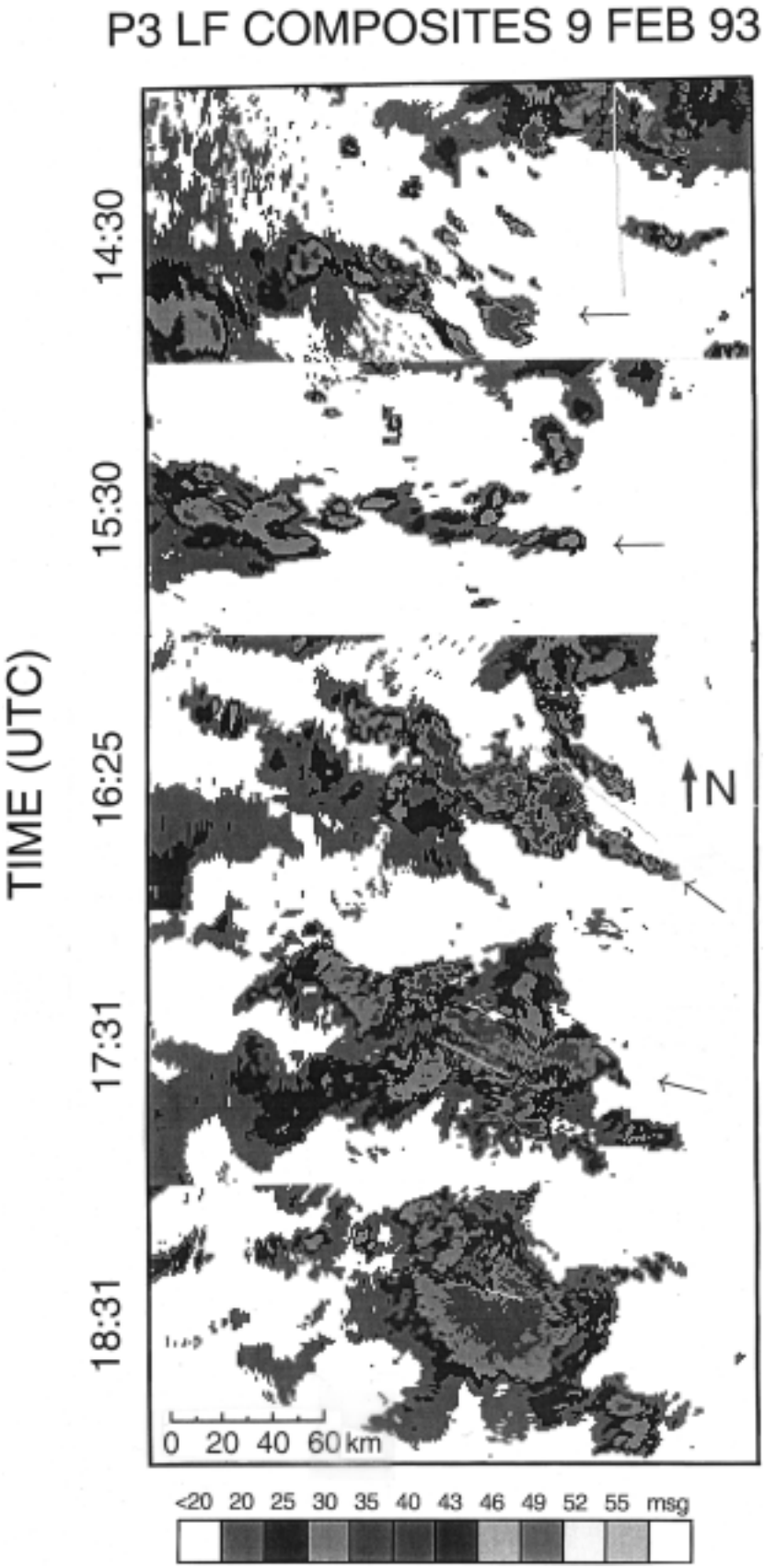

placement of the system (as defined by cloud-top temperature less than 208 K) in 12 h, equivalent to a westward speed of 6 m s^{-1}. In contrast, analysis of high-time-resolution radar images yields a line motion toward 020° about 8 m s^{-1} at 1620 UTC, within ± 2 m s^{-1} of the environmental low-level maximum line-normal wind component (LeMone et al. 1998). The line slowed with time, becoming nearly stationary by the time it dissipated at about 2000 UTC. According to Smull et al. (1994), convective features moved eastward along the line, and northward propagation was through growth of new convective cells. Although the time resolution in Fig. 6 is too poor to track features, one can discern the northward motion of the system through the period shown, and eastward movement of the eastern edge of the line before 1625 UTC, when it becomes stationary. The satellite-derived westward motion is intermediate between the motion measured within the convective system and advection by the wind in which the cloud tops were embedded (K. Y. Boyd 1994, personal communication; Boyd 1994). The satellite sequence does not suggest new convective cells forming to the west of the old convective clouds for this case.

2) 20 FEBRUARY CASE

Figure 7 shows the satellite IR-based Hovmöller diagram, and Fig. 8 is a sequence of lower-fuselage radar images from *NOAA-42* of a squall-line system that formed to the east of the IFA position on 20 February 1993. The squall line was oriented north–south, with trailing east–west convective bands near its north and south edges, and an extensive trailing stratiform region (Lewis et al. 1998).

The satellite sequence indicates the envelope of the region with cloud-top temperature less than 214 K shifted westward at ~10 m s^{-1}. There were three convectively active periods. The first was prior to 1822 UTC, the second between 1932 and 2332 UTC, and the third starting around 2432 UTC. Westward motion is slowed or interrupted during each period. Between 2032 and 2225 UTC, the eastern edge of the cloud shield, which indicates the location of the squall line (Rickenbach 1999, manuscript submitted to *Mon. Wea. Rev.*), moved eastward at 12 m s^{-1}, while the western edge remained stationary. Analysis of the radar images by Lewis et al. (1998) and Fig. 8 indicate that the squall line (indicated by an arrow in the figure) moved eastward at 12 m s^{-1}, the speed of the low-level jet in the environmental sounding. The reduction in the area of cold cloud between 2225 and 2332 UTC in Fig. 7 suggests that the system was rapidly weakening by 2332 UTC, when the westward cloud-shield motion resumed.

The resumption of westward motion in the satellite images was related to two factors, westward advection of high cloud, which dominated its motion when the squall line was clearly weakening, and the development of new convective cells to the west of the old system. Doppler analysis reveals east winds at echo-top height (12 km), and the environmental soundings show east winds above about 6 km (Lewis et al. 1998), consistent with westward motion of cloud material at higher levels. In addition, new convective cells started to form to the west of the old system at 2240 UTC (Fig. 8), which presumably contributed to the resurgence of cold cloud at 2432 (Fig. 7).

4. Discussion

The movement of the modeled and observed precipitating cloud systems can be interpreted in terms of dynamics of convection in shear as described by Moncrieff (1981), who identified two basic dynamical structures in organized convection: (i) the ''propagating'' structure where the anvil trails behind the cloud system and the highly organized convection moves in the same direction as, and at about the speed of, the jet maximum; and (ii) the ''steering-level'' structure in which the anvil cloud extends ahead. The former is common with an environmental wind profile that has a wind maximum at 1–3 km (i.e., shear reversal with height) while the latter tends to occur in unidirectional shear. The consequences in terms of the longevity of squall lines in distinct shear profiles was demonstrated in Thorpe et al. (1982) and Rotunno et al. (1988).

The time–height cross section of wind fields in Fig. 1 suggests that steering-level systems, with both precipitating clouds and anvil clouds moving westward,[1] are most likely during the first period (easterly wind period 10–17 December) (Fig. 3). With the exception of 16 December, the low-level jets in Fig. 1 are weaker and at lower altitudes than typically associated with shear-perpendicular convective bands with extensive precipitation (Alexander and Young 1992; LeMone et al. 1998). On the other hand, the wind field in Fig. 2 indicates that propagating systems, in which precipitating clouds move eastward while anvil clouds move westward, are most likely during the second period (westerly wind period, 20–27 December) (Fig. 4). Here, strong low-level jets exist in the westerlies ~75% of the time. Ship radar observations (LeMone et al. 1998) indicated several eastward-moving propagating-type squall lines with leading-edge and trailing-stratiform structure (e.g., Houze et al. 1990) during the westerly wind period.

The aircraft-observed cloud systems of Figs. 5–8 were both of the propagating type as defined by Moncrieff (1981). They moved with the line-normal component of the low-level wind maximum, which had an eastward component, and their anvils spread rearward

[1] In this context, westward can be interpreted as having a significant westward component, while eastward can be interpreted as having a significant eastward component, i.e., northward or southward motion are not excluded.

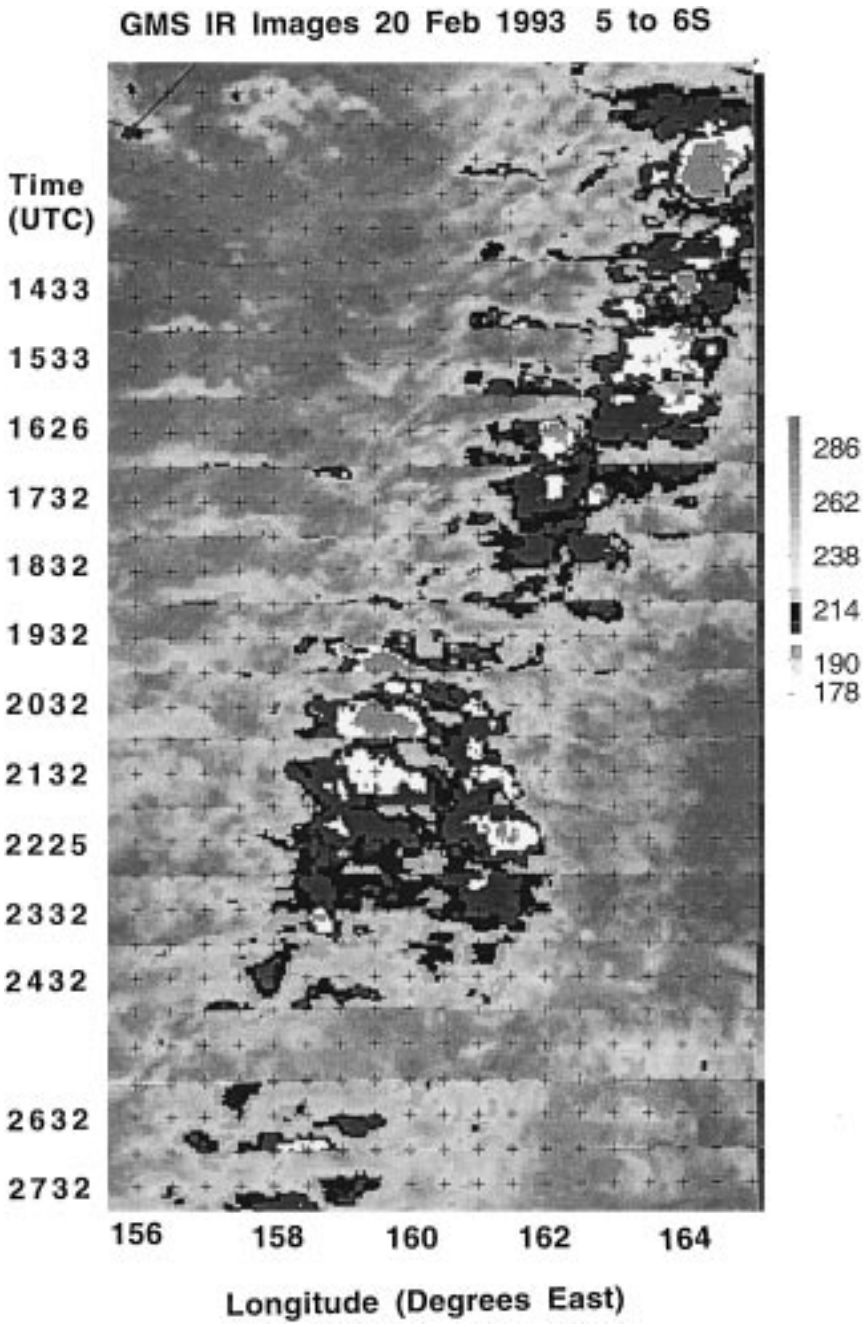

FIG. 7. 20 February GMS satellite IR-based Hovmöller diagram. Scale at right is infrared temperature in K. Aircraft investigation from ~1940 to 2620 UTC. A strip of satellite image with no high cloud has been inserted in the 2532 UTC position, since there is no satellite image for that time.

in the opposite direction. In the case of 20 February, the westward anvil growth corresponded to the environmental wind direction. However, the southwestward-growing anvil of 9 February was also stretched westward by the environmental wind. Furthermore, the lower-tropospheric westerly winds advected individual cells eastward along the convective band.

5. Summary

During the westerly wind periods in December 1992 and February 1993, both model-produced cloud-scale properties and observations show that precipitating convective cells move eastward, while the upper-tropospheric clouds move westward. The zonal wind in this

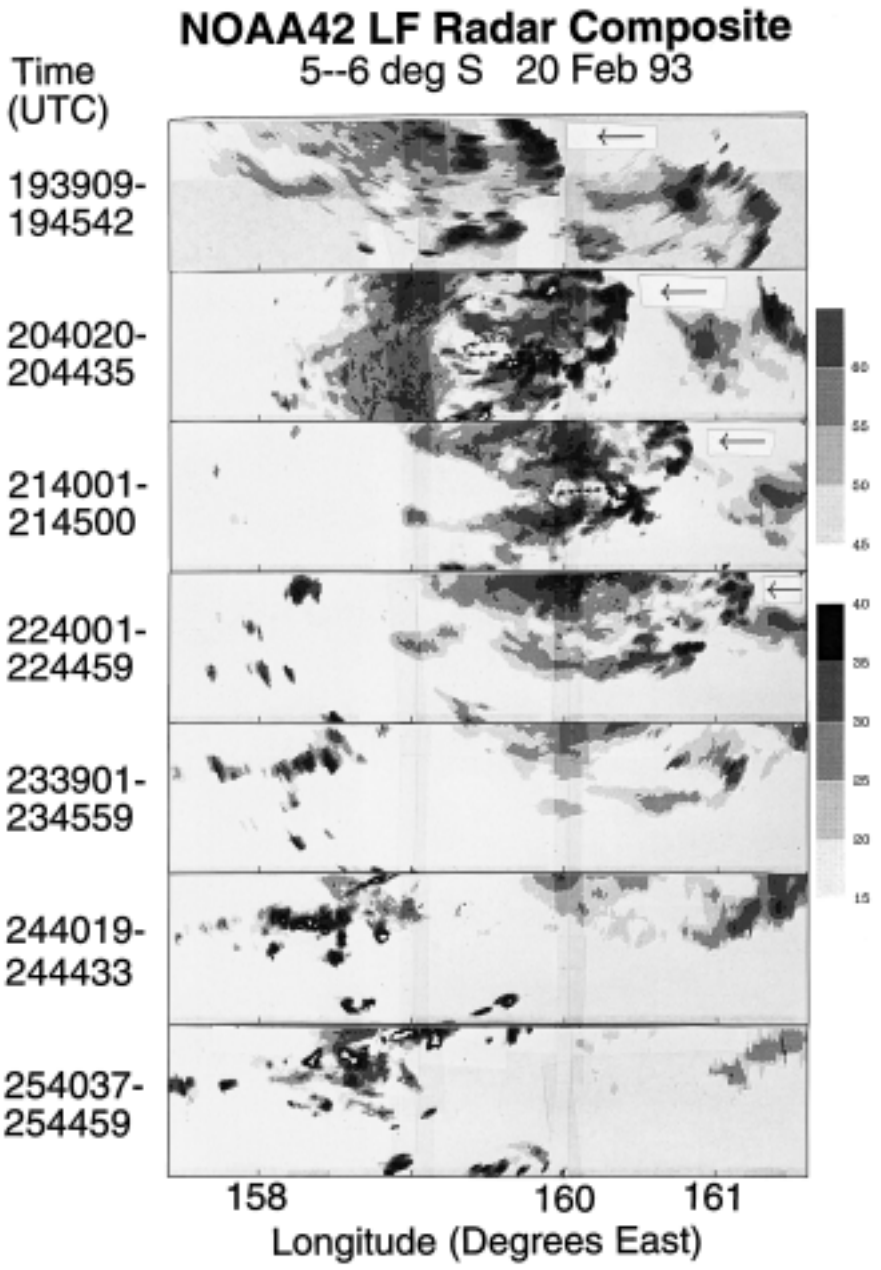

FIG. 8. As in Fig. 6 but for 20 Feb. Arrows indicate the squall line system in the top four frames. Reflectivity scale appears to the right. Note new convective cells forming to the west, the leading edge of which moves eastward at about the same speed as the squall line. Areas of slight darkening at 159° and 160°E are due to tape.

phase of the intraseasonal oscillation in TOGA COARE typically had a low-level maximum at 1–3 km and westerlies through the lower troposphere (Fig. 2, also Lin and Johnson 1996), which governed the motion of the active precipitating clouds. The relationship of wind profiles to storm motion is well established; it has been discussed theoretically (e.g., Moncrieff 1981; Thorpe et al. 1982; Rotunno et al. 1988) and documented in numerous observational studies for tropical mesoscale convective systems (e.g., Barnes and Sieckman 1984; Keenan and Carbone 1992; LeMone et al. 1998). The occasional apparent disconnect between satellite-tracked clouds and radar-tracked precipitations gives credence to the existence of two-day westward-propagating waves.

The movement of cloud patterns during TOGA COARE obtained in this note is consistent with other TOGA COARE observational studies. The analyses of

the cloud-resolving simulation, satellite, and radar data further refine Nakazawa's westward-moving disturbances to shorter time- and space scales. Understanding of the fine structure of cloud systems becomes important when atmosphere–ocean coupled models are used to study the mechanisms for the intraseasonal oscillation. Cloud systems strongly affect surface longwave, shortwave, latent heat, and sensible heat fluxes; and accurate surface forcing is crucial for the simulation of sea surface temperature.

Acknowledgments. The authors would like to thank Mitch Moncrieff for the discussion on this work. Sharon Lewis generously provided the radar and satellite images from which Figs. 7 and 8 were constructed. Personal reviews of the manuscript by Wojtek Grabowski, Ralph Milliff, Bill Rossow, and Stan Trier are gratefully acknowledged. Comments by Richard Johnson, Tom Rickenbach, and one reviewer greatly improved the presentation of results. This work was supported by the NSF Grant ATM-9525857 and is part of the NCAR Clouds in Climate Program.

REFERENCES

Alexander, G. D., and G. S. Young, 1992: The relationship between EMEX mesoscale precipitation feature properties and their environmental characteristics. *Mon. Wea. Rev.,* **120,** 554–564.

Barnes, G. M., and K. Sieckman, 1984: The environment of fast- and slow-moving tropical mesoscale convective cloud lines. *Mon. Wea. Rev.,* **112,** 1782–1794.

Betts, A. K., R. W. Grover, and M. W. Moncrieff, 1976: Structure and motion of tropical squall lines over Venezuela. *Quart. J. Roy. Meteor. Soc.,* **102,** 395–404.

Boyd, K. Y., 1994: Characteristics of superclusters over the western Pacific Ocean warm pool. NCAR 1994 Summer Employment Program, 23 pp. [Available from UCAR, P.O. Box 3000, Boulder, CO 80307.]

Chen, S. S., R. A. Houze Jr., and B. E. Mapes, 1996: Multiscale variability of deep convection in relation to large-scale circulation during TOGA COARE. *J. Atmos. Sci.,* **53,** 1380–1409.

Geldmeier, M. F., and G. M. Barnes, 1997: The ''footprint'' under a decaying tropical mesoscale convective system. *Mon. Wea. Rev.,* **125,** 2879–2895.

Haertel, P. T., and R. H. Johnson, 1998: Two-day disturbances in the equatorial western Pacific. *Quart. J. Roy. Meteor. Soc.,* **124,** 615–636.

Houze, R. A., Jr., B. F. Smull, and P. Dodge, 1990: Mesoscale organization of springtime rainstorms in Oklahoma. *Mon. Wea. Rev.,* **118,** 613–654.

Jorgensen, D. P., M. A. LeMone, and S. B. Trier, 1997: Structure and evolution of the 22 February 1993 TOGA COARE squall line: Aircraft observations of structure, circulation, and near-surface energy fluxes. *J. Atmos. Sci.,* **54,** 1961–1985.

Keenan, T. D., and R. E. Carbone, 1992: A preliminary morphology of precipitation systems in tropical northen Australia. *Quart. J. Roy. Meteor. Soc.,* **118,** 283–326.

Lau, K.-M., P. Li, C.-H. Sui, and T. Nakazawa, 1989: Dynamics of super cloud clusters, westerly wind bursts, 30–60 day oscillations and ENSO: An unified view. *J. Meteor. Soc. Japan,* **67,** 205–219.

——, T. Nakazawa, and C.-H. Sui, 1991: Observations of cloud cluster hierarchies over the tropical western Pacific. *J. Geophys. Res.,* **96,** 3197–3208.

LeMone, M. A., G. M. Barnes, and E. J. Zipser, 1984: Momentum flux by lines of cumulonimbus over the tropical oceans. *J. Atmos. Sci.,* **41,** 1914–1932.

——, D. P. Jorgensen, and B. F. Smull, 1994: The impact of two convective systems on sea-surface stresses in COARE. Preprints, *Sixth Conf. on Mesoscale Processes,* Portland, OR, Amer. Meteor. Soc., 40–44.

——, E. J. Zipser, and S. B. Trier, 1998: The role of environmental shear and CAPE in determining the structure and evolution of mesoscale convective systems during TOGA COARE. *J. Atmos. Sci.,* **55,** 3493–3518.

Lewis, S. A., M. A. LeMone, and D. P. Jorgensen, 1998: Evolution and dynamics of a squall line that occurred on 20 February 1993, during TOGA COARE. *Mon. Wea. Rev.,* **126,** 3189–3212.

Lin, X., and R. H. Johnson, 1996: Kinematic and thermodynamic characteristics of the flow over the western Pacific warm pool during TOGA COARE. *J. Atmos. Sci.,* **53,** 695–715.

Moncrieff, M. W., 1981: A theory of organized steady convection and its transport properties. *Quart. J. Roy. Meteor. Soc.,* **107,** 29–50.

Nakazawa, T., 1988: Tropical super clusters within intraseasonal variations over the western Pacific. *J. Meteor. Soc. Japan,* **66,** 823–839.

Rickenbach, T. M., and S. A. Rutledge, 1998: Convection in TOGA COARE: Scale, morphology and rainfall production. *J. Atmos. Sci.,* **55,** 2715–2729.

Rotunno, R., J. B. Klemp, and M. L. Weisman, 1988: A theory for strong, long-lived squall lines. *J. Atmos. Sci.,* **45,** 463–485.

Smull, B. F., D. P. Jorgensen, T. J. Matejka, and M. A. LeMone, 1994: Evolution of precipitation and momentum structure within a slow-moving convective band observed by airborne Doppler radar during TOGA COARE. *Proc. Sixth Conf. on Mesoscale Processes,* Portland, OR, Amer. Meteor. Soc., 21–23.

——, T. J. Matejka, and M. A. LeMone, 1996: Airflow trajectories within a slow-moving convective system observed during TOGA COARE. *Proc. Seventh Conf. on Mesoscale Processes,* Reading, United Kingdom, Amer. Meteor. Soc., 289–290.

Sui, C.-H., and K.-M. Lau, 1992: Multiscale phenomena in the tropical atmosphere over the western Pacific. *Mon. Wea. Rev.,* **120,** 407–430.

Takayabu, Y. N., 1994: Large-scale cloud disturbances associated with equatorial waves. Part II: Westward-propagating inertio-gravity waves. *J. Meteor. Soc. Japan,* **72,** 451–465.

——, K.-M. Lau, and C.-H. Sui, 1996: Observation of a quasi-two-day wave during TOGA COARE. *Mon. Wea. Rev.,* **124,** 1892–1913.

Thorpe, A. J., M. J. Miller, and M. W. Moncrieff, 1982: Two-dimensional convection in non-constant shear: A model of mid-latitude squall lines. *Quart. J. Roy. Meteor. Soc.,* **108,** 739–762.

Trier, S. B., W. C. Skamarock, M. A. LeMone, D. B. Parsons, and D. P. Jorgensen, 1997: Structure and evolution of the 22 February 1993 TOGA COARE squall line: Numerical simulations. *J. Atmos. Sci.,* **54,** 386–407.

Velden, C. S., and J. A. Young, 1994: Satellite observations during TOGA COARE: Large-scale descriptive overview. *Mon. Wea. Rev.,* **122,** 2426–2441.

Wu, X., W. W. Grabowski, and M. W. Moncrieff, 1998: Long-term behavior of cloud systems in TOGA COARE and their interactions with radiative and surface processes. Part I: Two-dimensional modeling study. *J. Atmos. Sci.,* **55,** 2693–2714.

——, W. D. Hall, W. W. Grabowski, M. W. Moncrieff, W. D. Collins, and J. T. Kiehl, 1999: Long-term behavior of cloud systems in TOGA COARE and their interactions with radiative and surface processes. Part II: Effects of ice microphysics on cloud–radiation interaction. *J. Atmos. Sci.,* **56,** 3177–3195.

Yuter, W. E., R. A. Houze Jr., B. F. Smull, F. D. Marks Jr., J. R. Dougherty, and S. R. Brodzik, 1995: TOGA COARE aircraft mission summary images: An electronic atlas. *Bull. Amer. Meteor. Soc.,* **76,** 319–328.